Air Motions and Precipitation Structure of an Early Summer Squall Line over the Eastern Tropical Atlantic

ROBERT A. HOUZE, JR., AND EDWARD N. RAPPAPORT[1]

Department of Atmospheric Sciences, University of Washington, Seattle, WA 98195

(Manuscript received 18 May 1983, in final form 3 October 1983)

ABSTRACT

The 28 June 1974 squall line over the ship array of the Global Atmospheric Research Programme's Atlantic Tropical Experiment (GATE) has been examined. Aircraft, radar, satellite, sounding and surface data have been employed in the analysis. This squall line is the third GATE oceanic squall line to have been subjected to intensive case study analysis. The vertical air motions and the relative amounts of convective and stratiform rain in this case were similar to those of the other two lines. However, this squall line moved more slowly, without discrete jumps, and the horizontal airflow relative to the system was quite different from that associated with the other two lines. Except at the surface, the strong front-to-rear relative flow normal to the line observed at most levels in the other cases was absent, with the relative flow tending instead to be parallel to the line. In the low to middle troposphere, relative flow parallel to the line from the north fed a post-squall mesoscale downdraft. In the middle to upper troposphere, relative flow parallel to the line from the south fed a post-squall mesoscale updraft. This upper-tropospheric relative flow from the south turned northwestward across the squall line and apparently advected enough condensate forward to produce a radar echo overhang and stratiform rain area ahead of the squall line.

1. Introduction

The Global Atmospheric Research Programme's Atlantic Tropical Experiment (GATE) afforded excellent documentation of several tropical squall lines. These squall lines are mesoscale convective systems that distinguish themselves from other tropical cloud systems by their organization of deep convection into a rapidly propagating line (Houze and Betts, 1981). During GATE, which extended over the summer of 1974, six oceanic squall lines occurred over the primary GATE ship array (located in the eastern tropical Atlantic): four during late summer (4, 11, 12 and 16 September), one during midsummer (9–10 August) and one in early summer (28 June). Only two of these cases, the late summer squalls of 4 and 12 September, have been reported in detail (Zipser, 1977; Houze, 1977; Gamache and Houze, 1982, 1983). A distinct danger exists in generalizing too much from this limited sample of case studies.

The two GATE oceanic squall systems reported on so far both exhibited a trailing region of stratiform cloud and precipitation with little or no mid- or upper-level cloud extending ahead of the squall lines. Hamilton and Archbold (1945), however, pointed out that pilot reports suggested that stratiform cloud and rain extended ahead of some tropical squall lines, and they speculated that this might be the result of a quite different relative flow pattern than in other squall systems. If such differences exist, then overly generalizing from the two cases presented to date is indeed a possibility.

In this paper, we present a case study of the early summer squall line of 28 June. We show that this squall line was of the type referred to by Hamilton and Archbold, in that it exhibited a pre-line overhang of clouds. From GATE data, we determine this system's similarities to and its differences from the two previously described GATE oceanic squall lines. In particular, we will show that while the vertical air motions and the relative amounts of convective and stratiform rain in this case were similar to those of the other two squall systems, the mesoscale horizontal motions associated with the 28 June squall line differed markedly from those of the other squalls, one effect of the different horizontal motions being the production of the pre-line cloud and precipitation.

2. Data

Data in this study were obtained by 14 ships positioned as shown in Fig. 1 and by seven aircraft flying at the altitudes and times indicated in Table 1. Characteristics of surface, upper-air and radar observations provided by the ships are presented in detail in Rappaport (1982). All the aircraft except the US CV-990 (which provided the dropwindsondes at D_1 and D_2 in Fig. 1) flew generally along the track shown by the dashed line in Fig. 1. The squall system was located

[1] Present affiliation: Atmospheric Sciences Group, Texas Tech University, Lubbock, TX 79409.

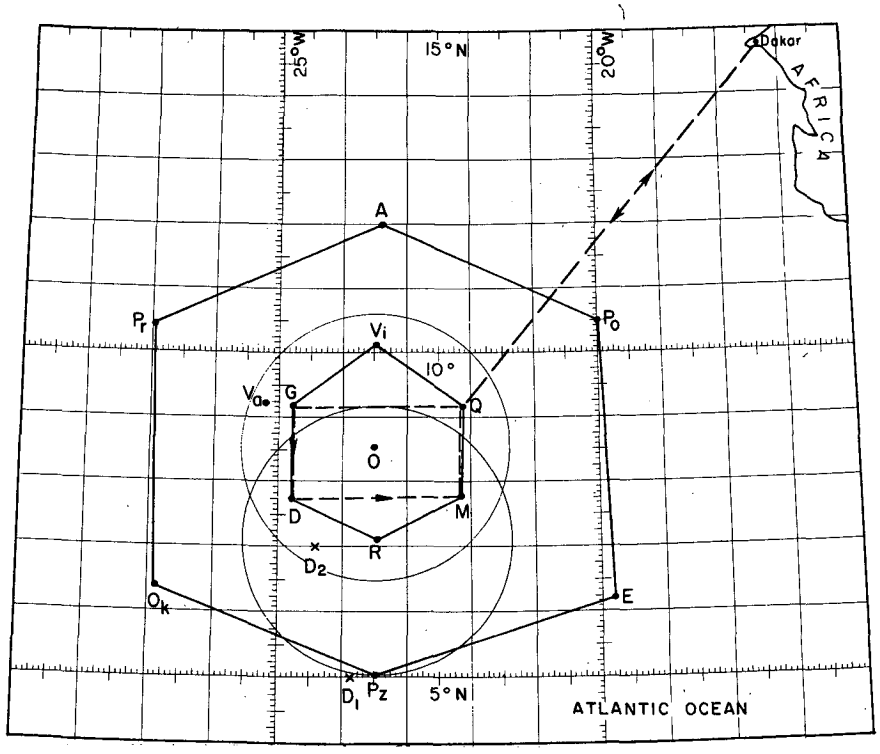

FIG. 1. GATE observational area on 28 June 1974. Hexagons represent B (inner) and A/B (outer) ship networks; D_1 and D_2 are dropwindsonde positions. Other capital letters indicate ship positions; circles indicate areas covered by *Oceanographer* (O) and *Researcher* (R) radars; dashed line shows flight track of research aircraft.

within the areas covered by radars on the ships *Oceanographer* and *Researcher* (overlapping circles in Fig. 1) and within the rectangle formed by the southern part of the flight track.

The dense set of data collected by ship and aircraft was complemented by imagery from the geosynchronous meteorological satellite SMS-1. Visible and infrared satellite pictures (1–7 km resolution) were obtained through the GATE Data Catalog,[2] and 23 km resolution maps of blackbody temperature were derived from infrared data archived at the National Center for Atmospheric Research by Smith *et al.* (1979).

3. Horizontal distribution of precipitation and cloud cover

The 28 June squall line appeared shortly after 0000[3] and lasted until about 2100. Fig. 2 contains overlaid quantitative satellite and radar imagery for three representative times. The position of the squall line is indicated by the heavy line at each time. The leading edge of a squall line is usually considered to be the surface windshift line (the "gust front" or "squall front"). Typically, the windshift line is close to (usually just ahead of) the leading edge of the heavy convective rain from the deep cells located along the squall line (e.g., Zipser, 1969, 1977; Houze, 1977). The position of the line was approximated here by the leading edge of the intense convective radar-echo zone that propagated through the region shown. The echo-intensity thresholds used to help identify the line are given in the figure caption. The squall line positions obtained

TABLE 1. Data pertaining to flights by GATE research aircraft on 28 June 1974.

Aircraft	Assigned flight level (mb)	Period of observation used in this study (GMT)	Temporal resolution of data
US DC-6	997	1200–1535	1 s
US L-188	970	1400–1415	1 s
UK C-130	845	1215–1750	1 s
France DC-7	700	1240–1750	10 min
US C-130	500	1700–1815	1 s
USSR IL-18C	400	1100–1630	variable (1–10 min)
US CV-990	240	1155–1540	1 s

[2] Available from the World Data Center A, National Climatic Center, Asheville, NC 28801.

[3] All times GMT, which over the GATE ship array corresponded approximately to LST plus 1.5 h.

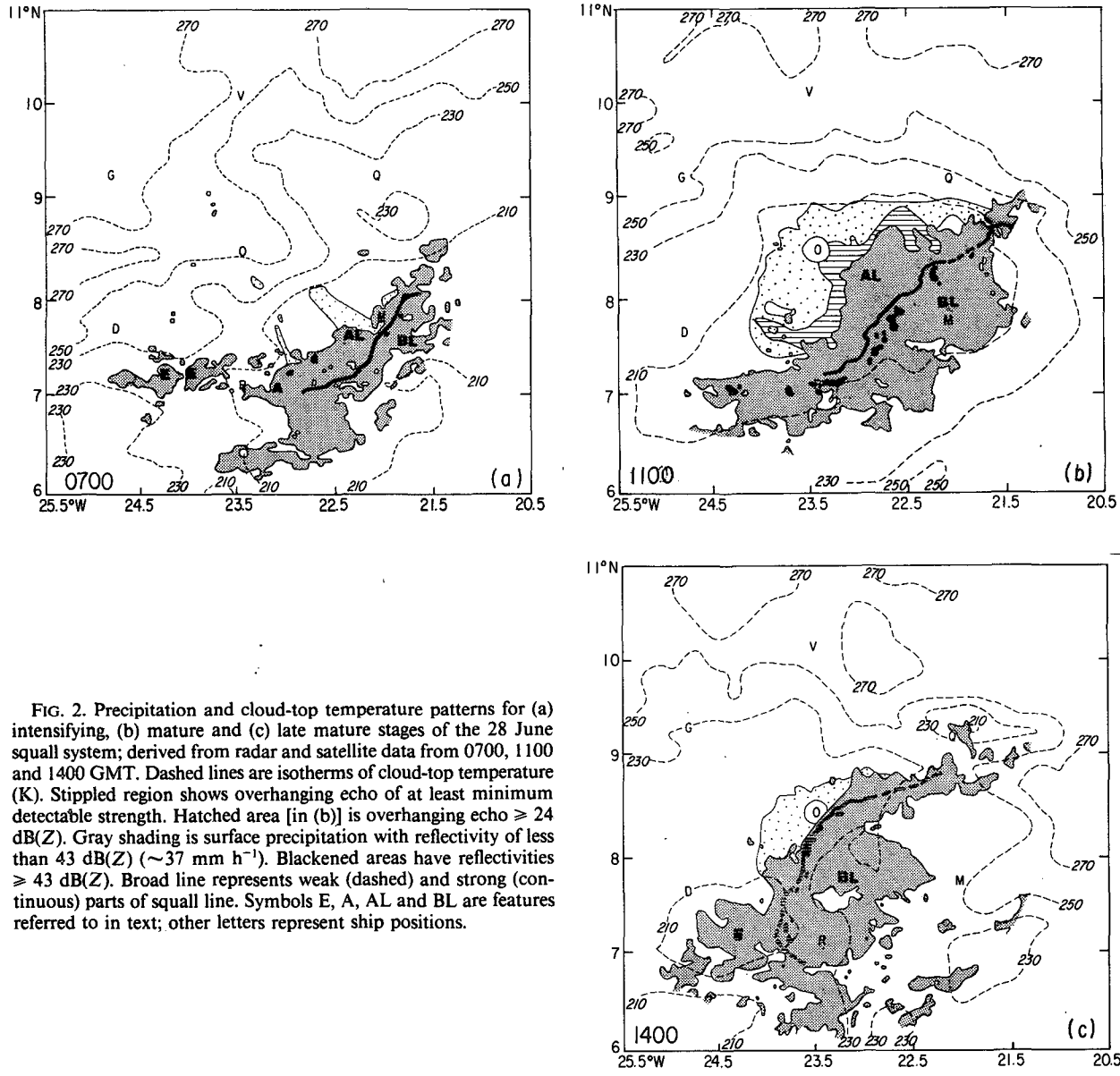

FIG. 2. Precipitation and cloud-top temperature patterns for (a) intensifying, (b) mature and (c) late mature stages of the 28 June squall system; derived from radar and satellite data from 0700, 1100 and 1400 GMT. Dashed lines are isotherms of cloud-top temperature (K). Stippled region shows overhanging echo of at least minimum detectable strength. Hatched area [in (b)] is overhanging echo $\geq$ 24 dB(Z). Gray shading is surface precipitation with reflectivity of less than 43 dB(Z) (~37 mm h^{-1}). Blackened areas have reflectivities $\geq$ 43 dB(Z). Broad line represents weak (dashed) and strong (continuous) parts of squall line. Symbols E, A, AL and BL are features referred to in text; other letters represent ship positions.

in this way were consistent with wind reports from all ships passed over by the line and all low-flying aircraft that crossed the line.

At 0700 (Fig. 2a), the squall line was entering the inner hexagon (B array) of GATE ships from the east-southeast; the line was located near the ship *Meteor* (M in the figure). The southern end of the line was interacting with a stationary west–east line of radar echo consisting at 0700 of the mesoscale rain areas labeled A and E. Stratiform rain areas extended a short distance ahead of (AL) and behind (BL) the squall line, and some areas of weak precipitation aloft (virga) were just becoming apparent ahead of the line at this time (stippled area in Fig. 2a). Area AL and the virga ahead of the line were associated with the pre-line overhang of cloud that developed in this case. Stratiform rain ahead was not found in previously analyzed GATE oceanic squall lines. An area of cloud-top temperature less than 210 K (greater than 13 km height) defined the central portion of the cloud shield that formed the top of the squall system at this time. The shield, like the stratiform rain, extended both ahead of and behind the squall line. Maximum tops of radar echoes along the squall-line convective zone were about 12 km at this time, and increasing. The tallest echoes of the day (about 17 km) occurred at 0930.

By 1100 (Fig. 2b), the squall system had reached its maximum areal coverage. The stratiform rain areas ahead and behind the line (AL and BL) had both expanded, and the virga extended forward, well past

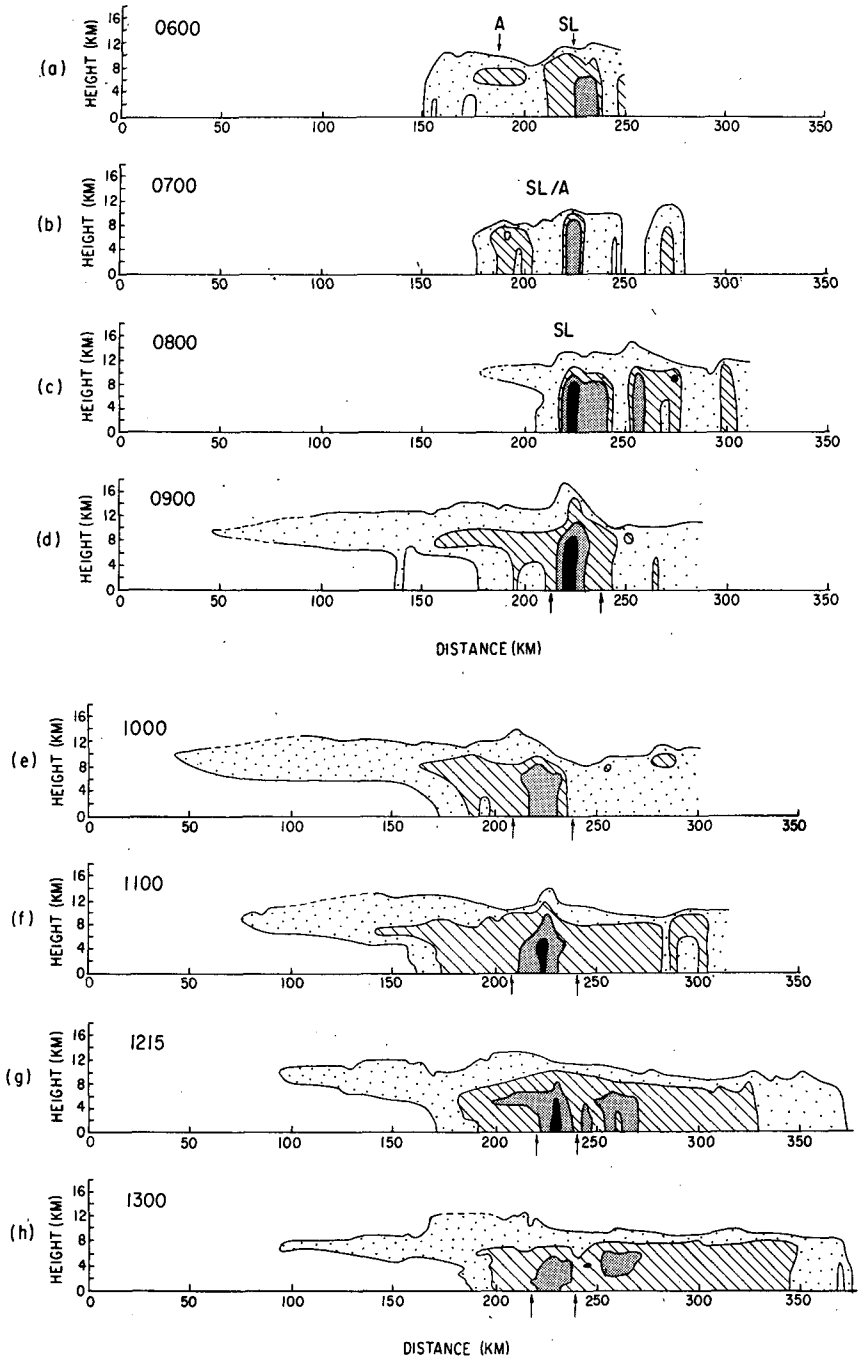

FIG. 3. Evolution of the vertical structure of squall system radar echoes. Cross sections are along propagation direction, with motion from right to left. Feature A and the squall line (SL) are identified during period of their interaction. Shading thresholds are for the minimum detectable, 24, 34 and 44 dB(Z). Small arrows denote front and back edge of convective zone discussed in Section 6.

Oceanographer, and had become more intense (see hatching in Fig. 2b). The convective cells along the squall line had begun to weaken (maximum tops about 15 km). However, the 210 K infrared isotherm continued to define the central core of the upper-level cloud shield. The outer edge of the cloud shield probably followed approximately the 230 or 250 K isotherm.

By 1400 (Fig. 2c), the system was weakening. The stratiform precipitation region ahead of the line had receded such that only some weak virga extending over *Oceanographer* remained. The stratiform rain area be-

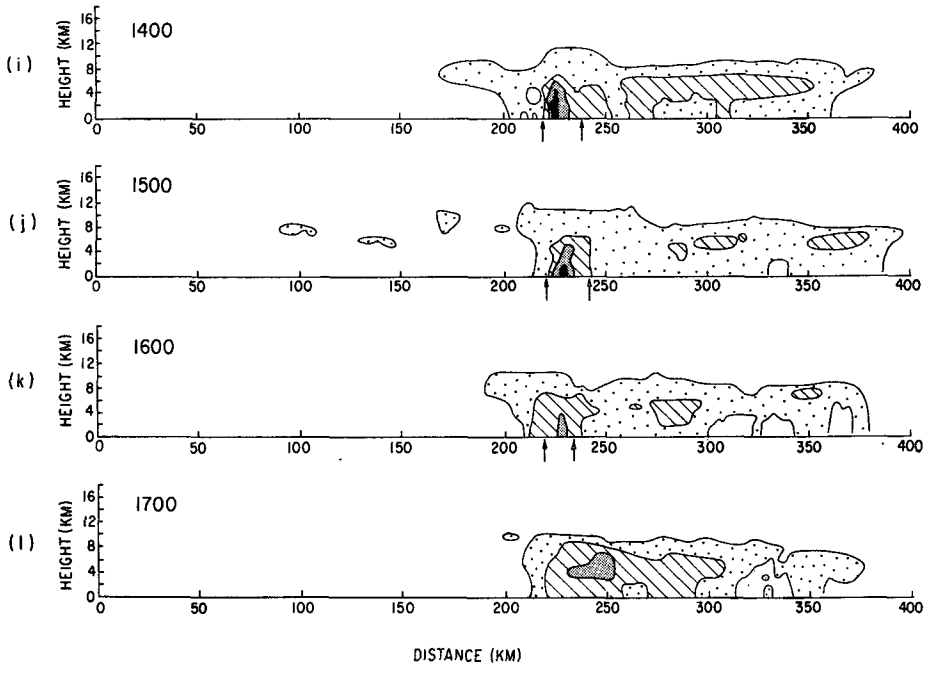

FIG. 3. (*Continued*)

hind the line (BL), however, persisted. Maximum cell tops along the squall line were only 9 km, and the only regions of cloud-shield temperature less than 210 K were over the mesoscale feature E ahead of the squall line and an isolated convective feature near the northern end of the line. The region of cloud-top temperature less than 230 K extended over and ahead of the line. The cloud top temperature over the trailing stratiform rain area had increased to between 230 and 250 K.

4. Vertical structure of the squall system

As seen in Figs. 2b–c, stratiform rain areas formed both ahead of (AL) and behind (BL) the squall line. The development of these features is further illustrated by the sequence of vertical cross sections of radar reflectivity in Fig. 3. These cross sections were taken normal to and near the center of the squall line. They are considered representative of their respective times. Exact locations of several of these sections are shown in plan view in Fig. 3.8 of Rappaport (1982).

At 0600 (Fig. 3a), the squall line was still becoming organized, and in the plan view the convective region consisted of cells in a roughly linear arrangement embedded within lighter precipitation. The pattern was complicated by the interaction with the pre-existing, slowly moving mesoscale rain area referred to as feature A in the figure.[4] The tops of the deepest convection at 0600 averaged about 12 km. The highest reflectivities were 35–45 dB(Z) (8–50 mm h^{-1}). The post-squall region appeared to be convective at this time, although it could not be characterized precisely since the squall line was far from the radar. The system appeared quite similar one hour later (Fig. 3b). Convection appeared to be a little more intense, with some 50 dB(Z) echoes being noted.

A dramatic change in vertical structure occurred between 0700 and 0900 (Fig. 3b–d). Convective cells along the squall intensified rapidly and grew to tower over all other precipitation. By 0900 the largest cells were over 16 km in height and often had low-level reflectivities between 45 and 51 dB(Z) (50–160 mm h^{-1}). The extensive region of stratiform echo aloft (virga) ahead of the squall line (i.e., the pre-line overhang referred to by Hamilton and Archbold, 1945) developed during this period. At 0900 it extended 175 km ahead of the line. This echo was thickest and most intense at its juncture with the squall line, gradually thinning out and becoming weaker with distance from the line. As the overhanging precipitation ahead of the line expanded, it gradually worked its way to the surface as "fingers" of light rain just ahead of the squall line (e.g., at 140 km and 180–210 km in Fig. 3d).

During the 0700–0900 period, the post-squall region contained scattered centers of weak to moderate convection in an otherwise stratiform radar echo pattern (Fig. 3c–d). The echo top in the post-squall region at 0900 was lower than the top of the pre-line echo overhang, and it remained so after this time.

Convective cells in the squall-line region reached their maximum heights and intensities at about 0900–

[4] The history of rain area A is described by Rappaport (1982).

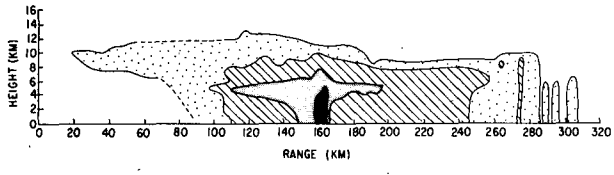

FIG. 4. Cross section showing stratiform rain and melting band ahead of and behind the squall line (located near 160 km) at 1215 GMT. Cross section is offset from propagation direction but is approximately normal to the line. Shading as in Fig. 3.

0930 (Fig. 3d) and the pre-line overhanging echo was most pronounced at 1000. After this time, the maximum cell heights declined and the overhang ahead of the squall line receded (Figs. 3e–g); however, the extent of the area of rain reaching the surface from the overhang just ahead of the line continued to increase. The greatest extent of this area was observed at 1100 (Fig. 3f; see also region AL in Fig. 2b) and 1215 (Fig. 3g).

During the late morning, the stratiform precipitation zone behind the line also became more extensive (Figs. 3e–g). The regions both ahead and behind the squall line began to exhibit radar bright bands in the melting layer. Though these bright bands are not seen well in Figs. 3f and g, except ahead of the line in Fig. 3g, they were quite evident in other cross sections at these times (e.g., Fig. 4).

The dissipation of the pre-squall stratiform precipitation and weakening of convection along the squall line can be seen in Fig. 3g–l. By 1400–1500, no cells along the line were greater than 8–9 km in height, and all that remained of the pre-squall stratiform precipitation was a small, patchy echo overhang. After 1700, neither a pre-squall echo nor convective cells along the line occurred.

The trailing stratiform region was also beginning to weaken in intensity at 1400–1500, but it remained extensive and continued to exhibit a strong bright band in the melting layer. From 1500 onward, absence of echo at low levels toward the rear of the system indicated evaporation of some of the trailing stratiform precipitation by a lower tropospheric mesoscale downdraft of the type discussed by Zipser (1969, 1977), Houze (1977), and Gamache and Houze (1982, 1983). Despite this low-level evaporation, the trailing stratiform region persisted, and by 1700 this region was all that remained of the squall system (Fig. 3l).

5. Movement of the convective zone

As noted in Section 3, the progression of the squall line can be seen from isochrones of the leading edge

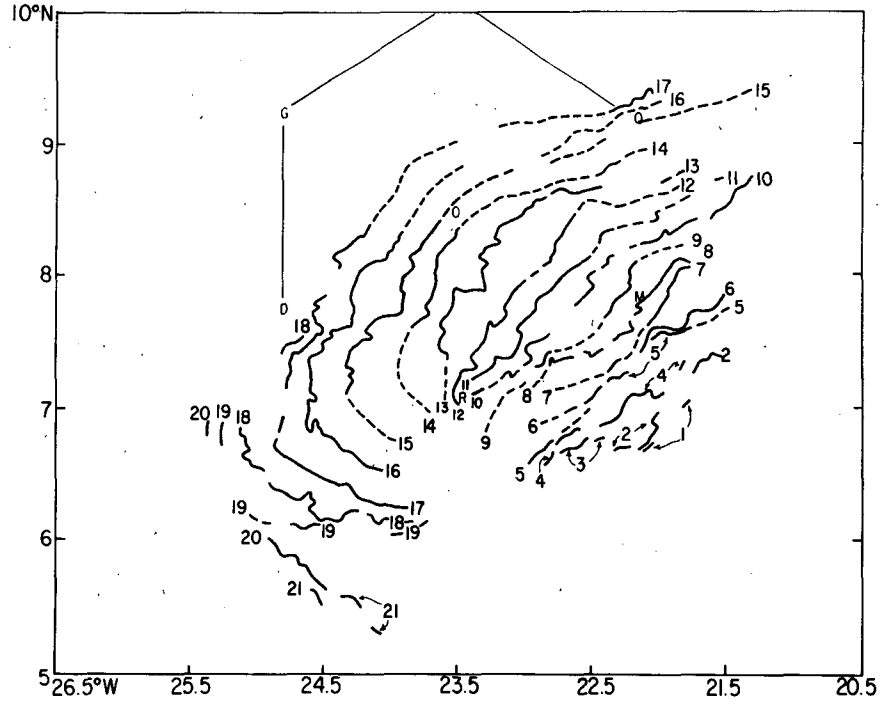

FIG. 5. Isochrones of leading edges of the lines of maximum precipitation rate associated with the squall line are labeled by hour of the day. Observations prior to 1200 were taken at 3 min past the hour; number 12 is the 1148 report. Positions denote leading edge of 31 dB(Z) (4 mm h^{-1}) echo during the pre-1100 and post-1400 periods and 39 dB(Z) (17 mm h^{-1}) during the interim period. The B array ship hexagon is also shown. Dashed segments show where the line was interpolated or extrapolated through weak or uncertain sections.

of the heavy precipitation constituting the propagating line of convective radar echo. These are shown in Figs. 5 and 6. Since some stratiform rain was located ahead of the 28 June 1974 squall line, the leading edge of the heavy rain had to be distinguished from the background precipitation ahead of the line. Before 1100 and after 1400, the 31 dB(Z) (4 mm h^{-1}) contour was used to indicate this leading edge; between 1100 and 1400, the 39 dB(Z) (17 mm h^{-1}) threshold was used. The line was interpolated or extrapolated where discontinuities occurred in the line (dashed segments in Fig. 5).

Generally, the squall line moved less rapidly (about 7 m s^{-1} on average) than the two lines analyzed previously by Houze (1977), Zipser (1977) and Gamache and Houze (1982, 1983). Those lines moved at 10–14 m s^{-1} during their early and mature stages. The slower movement of this line was a factor leading to a different pattern of system-relative horizontal airflow in this case.

From 0100–1300, the squall line steadily elongated and moved toward the northwest. After 1300, the northern portion of the squall line weakened progressively and advanced west-northwestward, while significant new growth occurred on the southern end of the line. After 1700, the new growth on the south was all that remained. This portion of the line, which moved toward the southwest, was treated as a separate squall line in the thesis of Rappaport (1982). The formation and movement of the southern line segment is illustrated in more detail in Fig. 6. The original squall line is labeled SL; the new segment, called N, appeared at 1400 at a considerable distance from the position of SL at 1300. At 1600, SL and N had merged to form one line again, then they reseparated at 1800 when SL was dying, but N was still fairly strong.

Propagation by irregular pulses or jumps is a commonly observed behavior in squall lines. This line did not exhibit discrete jumps by small-scale (10–50 km long) squall line elements as did the 4 September GATE squall line (Houze, 1977). However, the sudden formation of the larger (100 km long) segment N was reminiscent of the triggering of new squall lines ahead of older ones, noted by both Houze (1977) and Fortune (1980). Also, two or three transient accelerations of squall-line segments occurred. They can be seen at 23°W, 8°N between 1200 and 1400, at 24°W, 7.5°N between 1400 and 1600, and possibly at 24.5°W, 6°N between 1900 and 2000. Each of these arc-shaped pulses is marked by an acceleration of the isochrones of the line after which the convection seems to stall and weaken.

If this squall line had exhibited discrete propagation, its net horizontal motion would have exceeded 7 m s^{-1}, and a system-relative airflow more like that of the previously described GATE squall lines might have occurred. The forward overhang diverging out of the tops of the cumulonimbus cells located along the squall line might then have been in part "bitten off" by the discrete jumps of the propagating line, thereby always finding itself behind the current active line.

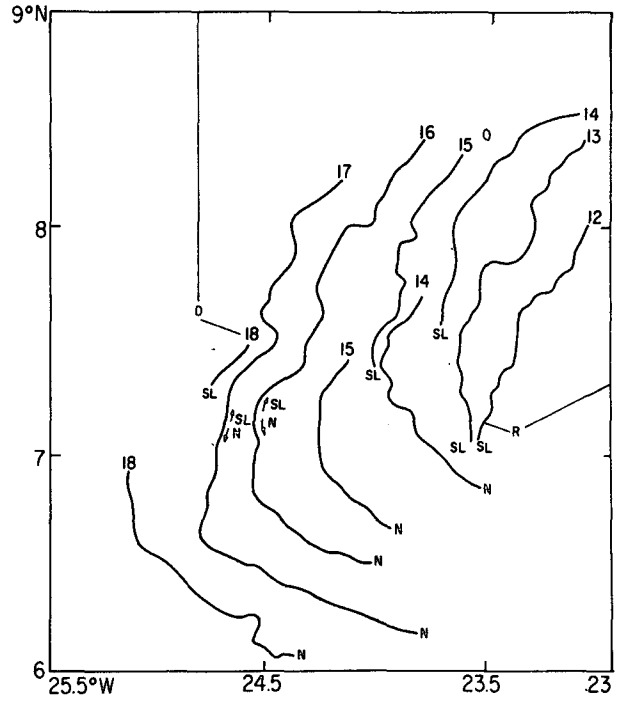

FIG. 6. Detailed isochrone pattern showing formation of line segment N.

6. Evolution of the total precipitation and cloud cover

To discuss total precipitation, the squall system is divided into four sections: the stratiform regions ahead of the squall line (AL) and behind the line (BL), the convective band comprising the original squall line (SL), and the squall-line segment (N), which developed late in the lifetime of the system at the southern end of SL (Fig. 6). The regions AL, BL, SL and N were

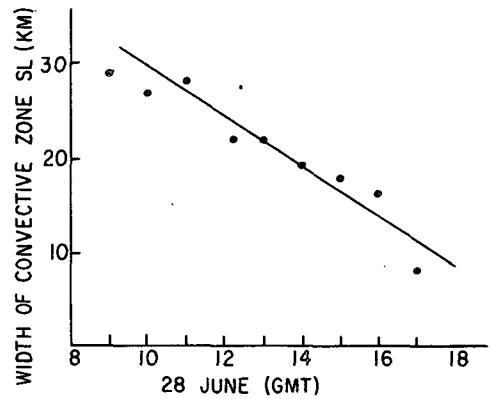

FIG. 7. Temporal variation of width of convective zone.

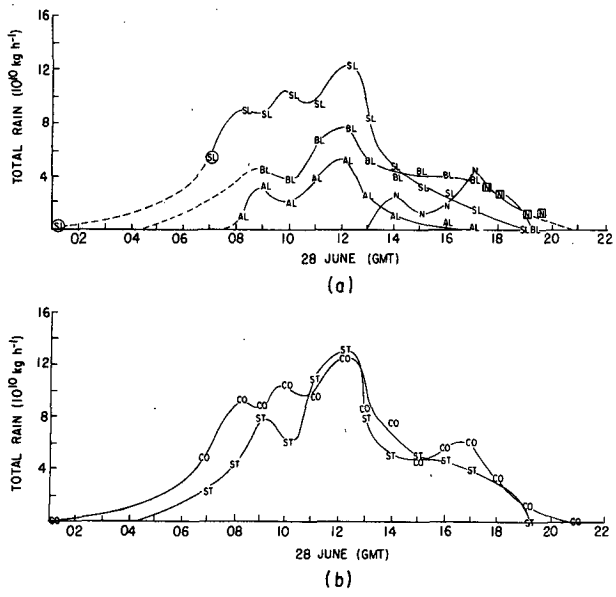

FIG. 8. (a) Variation in time of area integrated total rainfall in regions SL, N, AL and BL (defined in text). Data points derived from *Oceanographer* radar are encircled. Points from *Researcher* echoes are enclosed by squares. Remainder of data points are from composite *Researcher* and *Oceanographer* echo patterns [Composite echo maps were made by superimposing the patterns detected simultaneously by *Researcher* and *Oceanographer*. In the case of differing reflectivities, the higher dB(Z) was chosen. A similar technique was used by Houze (1977)]. (b) As in (a), except for total convective (CO = AL + N) and total stratiform (ST = AL + BL) rainfall.

identified in radar-echo patterns by locating the front and back edges of the convective bands corresponding to SL and N. Region AL consisted of all the rain ahead of the leading edges of the convective zone, while BL consisted of all the rain behind the trailing edges of the convective zones. The leading edges of the convective zones were obtained by connecting the leading edges of the line elements contained in the squall-line segments SL and N. This leading edge closely corresponded to the isochrones in Figs. 5 and 6. The back edge of the squall-line segment N was fixed at 20 km behind the leading edge. The back edge of SL was located beyond the rear border of the line elements, at the spot where echoes became intermediate between convective and stratiform. This point, determined somewhat subjectively, was the one which most clearly marked the onset of: 1) uniform echo tops, 2) moderate rainfall rates [radar reflectivity factor less than 35 dB(Z)], 3) small gradients of rainfall rate in both the horizontal [not exceeding $\sim$1 dB(Z) km^{-1}] and vertical. At this demarcation, over the period 0900–1700, the echoes had an average low-level radar reflectivity factor of 27 dB(Z) [2 mm h^{-1}; 70% of the echoes were between 25 and 33 dB(Z)] and average tops of 10 km (ranging from 8–13 km). Behind this demarcation, vertically oriented echoes, or echoes exceeding those at the demarcation by more than 3 dB(Z) in intensity were rare. The arrows in Figs. 3d–k show the front and back boundaries of the convective zone in those particular cross sections. From Fig. 3 and other cross sections, the mean width of the convective zone was determined as a function of time (Fig. 7). The width was greatest at about 0900 when the convective cells along the squall line were deepest and most intense (Fig. 3).

Instantaneous patterns of low-level rainfall rate indicated by radar were integrated over the areas of each region (SL, N, AL and BL) to obtain the curves in Fig. 8a. The GATE $Z - R$ relationship of Hudlow *et al.* (1979), $Z = 230R^{1.25}$, where Z is the equivalent radar reflectivity factor in mm^6/m^{-3} and R is rainfall rate in mm h^{-1}, was used. Precipitation associated with rain areas in the vicinity of but not part of the squall system was excluded from the totals (e.g., the areas A and E seen in Fig. 2a). Fig. 8a shows that rainfall gradually increased in SL, AL, and BL during the morning, with the greatest rainfall in SL and the least in AL. All three regions produced their maximum rainfall at 1200. Total rain quickly diminished in AL

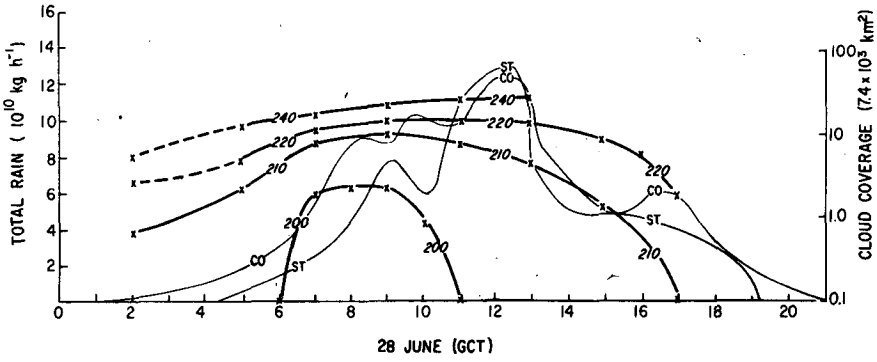

FIG. 9. Cloud coverage (heavy lines) derived for the squall system from infrared cloud-top temperatures and precipitation distribution (thin lines) obtained from Fig. 8. Coverage by 200, 210, 220 and 240 K cloud-top temperature isotherms is shown on a logarithmic scale, with crosses denoting data points. Dashed lines indicate extrapolations.

and SL during the afternoon; precipitation in BL decreased much more slowly. More rain fell in BL than SL after 1400. This persistence of the rainfall behind the squall line was aided by the formation of a mesoscale updraft in the trailing mid-upper tropospheric stratiform cloud. This mesoscale updraft is documented by wind data in Section 17.

The total stratiform rainfall from the squall system, obtained by combining the precipitation of regions AL and BL, and the total convective rainfall obtained by combining the precipitation of regions SL and N, are shown in Fig. 8b. The two curves are nearly parallel, with slightly more rain falling in convective zones at most times. Both curves rise gradually to a peak near noon and then gradually drop off. Integration of the curves in Fig. 8b with respect to time shows that approximately 1.8×10^{-12} kg of rain fell from the squall system, with 58% of the precipitation being convective and 42% stratiform. (About three-fourths of the stratiform rain fell from BL, with the remainder occurring in AL.) This percentage of stratiform rain is similar to the 40% found by Houze (1977) for the 4 September GATE squall line and the 49% found by Gamache and Houze (1983) for the 12 September GATE squall line.

Curves showing the total area covered by cloud tops with infrared temperatures below 200, 210, 220 and 240 K are superimposed on the total rainfall curves in Fig. 9. The period during which cloud-top temperatures less than 200 K occurred (0600–1100) was relatively brief and early in the development of the squall system. This period coincided with the occurrence of the deepest and most intense cells observed on radar (cf. Fig. 3d). The convective zone on radar was also widest at this time (Fig. 7). The extremely high cloud tops disappeared well before the system produced its maximum rainfall (around 1200). There appears to be a natural tendency for the most intense convective cells to occur early in the life cycle of mesoscale cloud systems (Maddox, 1980; Churchill and Houze, 1984).

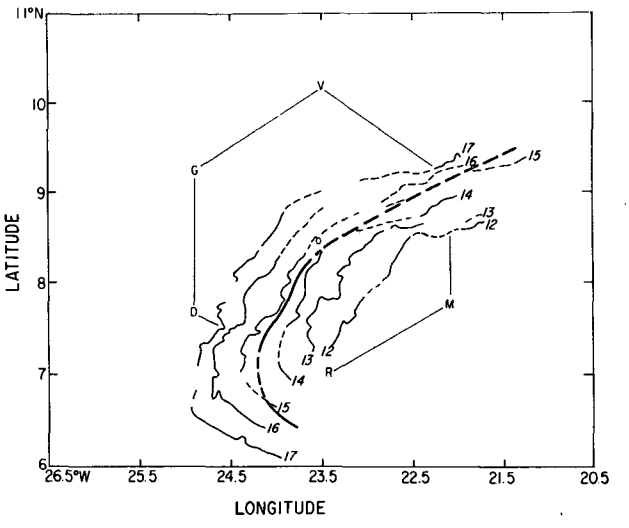

FIG. 10. Squall-line representation (heavy line) used for afternoon composite, and 1200–1700 GMT isochrones from which it was derived.

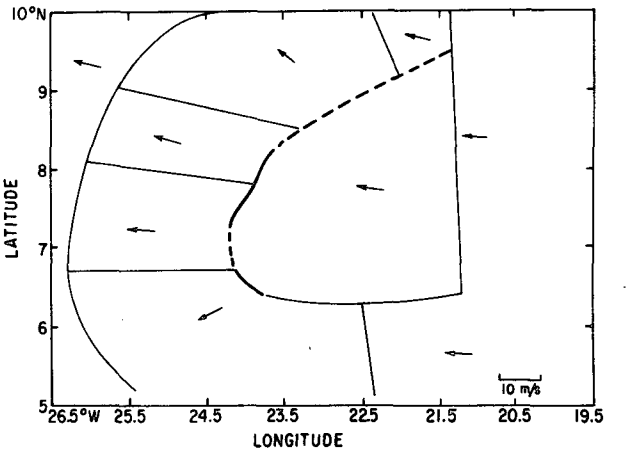

FIG. 11. Afternoon composite squall-line representation (wide line) and subdivided analysis region.

The infrared satellite data in Fig. 9 further show that the area and duration of the cloud shield easily satisfy the criteria used by Maddox (1980) to identify "mesoscale convective complexes (MCCs)". According to these criteria, the cloud top must exhibit continuously low infrared temperature less than or equal to 241 K, over an area of at least 10^5 km^{-2} and an interior cold cloud region, where the temperature is less than or equal to 221 K over an area of 5×10^4 km^{-2}, for a period of 6 h or more.

7. Construction of mesoscale wind patterns

The mesoscale airflow surrounding the squall system during the afternoon of 28 June[5] was estimated by transferring wind observations to the positions they would have had at the middle of this time period. The mean position and shape of the squall line between 1200 and 1700 was obtained by overlaying isochrones of the squall line and drawing a curve that lay in the middle of the group (Fig. 10). This curve (positioned with respect to latitude and longitude as shown in Fig. 10) is referred to as the "composite line" and replotted in Fig. 11. The vectors in Fig. 11 indicate the motion of the squall line in various regions. The directions vary since the squall system tended to expand, and the propagation velocity was not constant along the squall line (cf. Fig. 5). Areas far from the line and in the post-squall region were assigned the mean squall

[5] A similar analysis was made for the morning but is not described here since the wind data for the morning period were not complete enough to allow calculation of mesoscale divergence and vertical motion. A discussion of the morning composite may be found in Rappaport (1982).

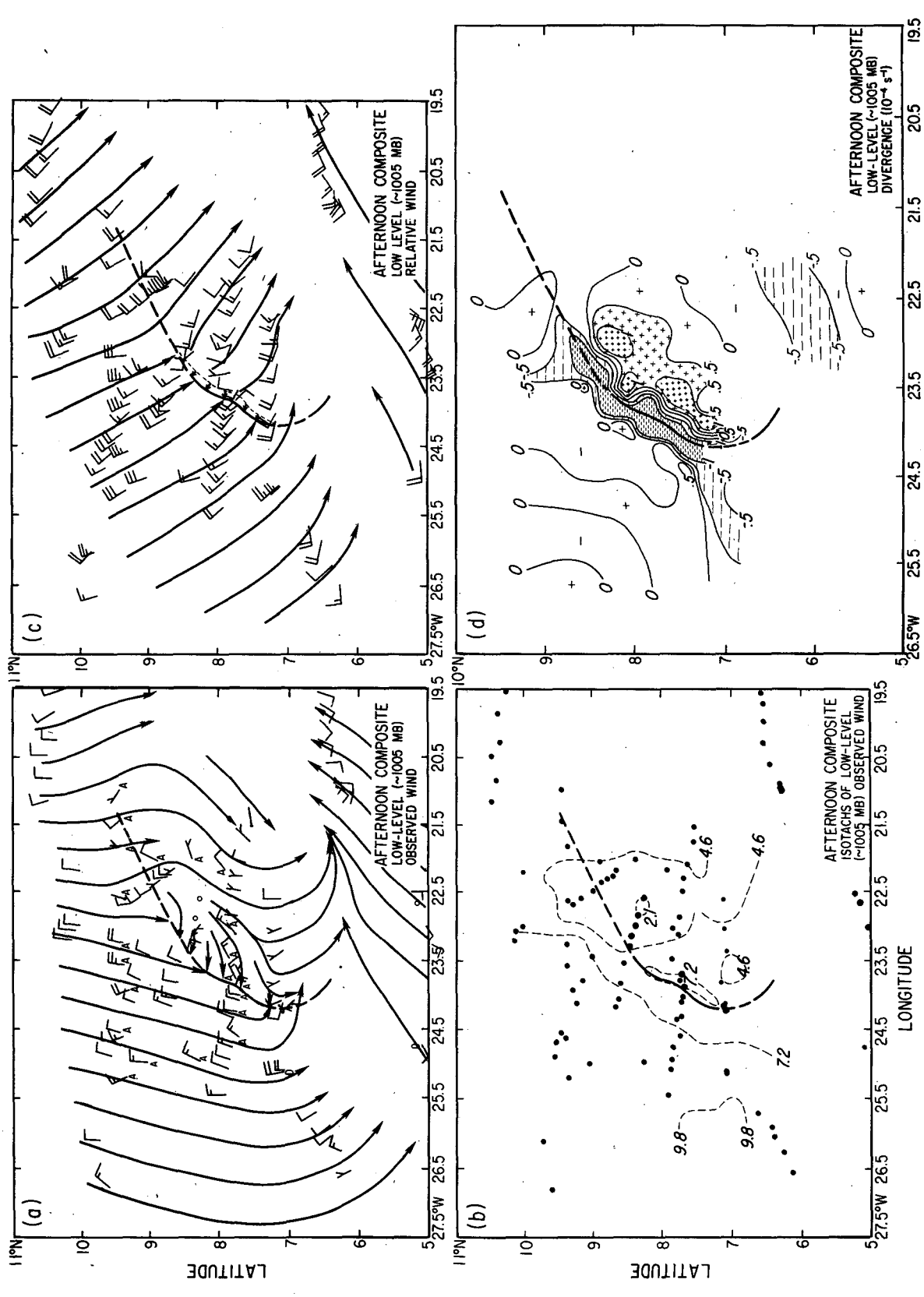

FIG. 12. Low-level wind analysis for afternoon composite. (a) Streamlines and plotted winds from aircraft (A), dropwindsonde (D) and ship observations; (b) isotachs (wind speed in m s^{-1}) with observation points shown by dots; (c) relative wind field, with dashed line showing estimated back edge of post-squall inflow region; (d) divergence in units of 10^{-4} s^{-1}. In (a) and (c) full barb is for 5 m s^{-1}, half barb for 2.5 m s^{-1} and 0 for calm wind. Composite squall-line position shown by heavy line.

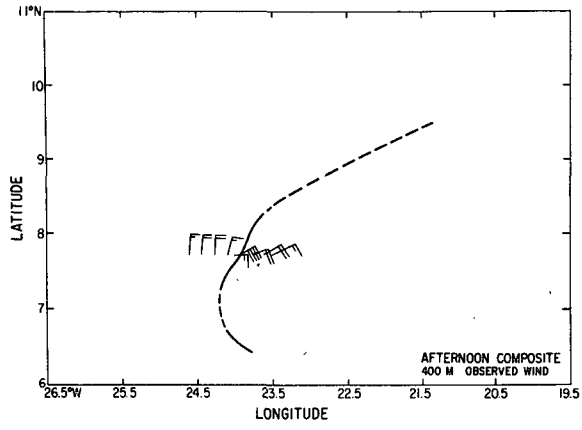

FIG. 13. Wind data obtained from L-188 aircraft flying at 400 m between 1400 and 1415 GMT. Composite squall-line position shown by heavy line.

line velocity (7 m s^{-1} from a direction 100 deg east of true north). For ships passed over by the squall line, the angle from which the line approached the ship defined a vector along which all the ship's data were plotted. The distance between sequential observations was determined by the speed of the squall line along this vector. Data obtained aboard aircraft, from dropwindsondes and from isolated ship measurements not part of a time series showing the squall-line passage were plotted by positioning each observation first, with respect to the squall-line isochrone for the time when the measurement was made. Then the observation was located relative to the composite line by matching the current isochrone to that of the smoothed composite line.

Once all the data were located relative to the smoothed composite line, streamlines and isotachs were drawn to determine the mesoscale flow in the vicinity of the line. This procedure differs from that used by Gamache and Houze (1982, 1983), who located observations relative to the central point of the squall line rather than with respect to the portion that passed over each measurement station. Consequently, details of structure along the squall line were blurred in their analysis. We preserve details near the line by positioning the observations at each platform crossed over by the squall line on the correct side of the line (ahead or behind) and at precisely the distances from the line at which the data were taken. As a result, narrow features, such as the gust front and the transition zone at the rear of the convective region are defined in our analysis.

After all wind data from various times were plotted on a map with the composite line, streamlines and isotachs of the observed winds were drawn [see panels (a) and (b) of Figs. 12, 14, 15, 17 and 18]. These maps estimate the flow surrounding the squall line at about the middle of the afternoon.

Divergence and vorticity fields were computed from interpolated grid-point values of the winds on these maps. The divergence patterns are shown in the (d) panels of Figs. 12, 14, 15, 17 and 18. The vorticity fields are not discussed here but may be found in Rappaport (1982).

In locating observations relative to the composite line, we assumed that the mesoscale wind field was in a steady state in a coordinate frame attached to the squall line. However, since the velocity of the squall line varied along the line (Fig. 11), the coordinate system itself was expanding. Consequently, the magnitude of divergence for a given subregion of the composite system decreased slightly in time, since the area of the subregion was increasing. The values of divergence obtained in our calculations apply when the system was the size it had reached at the middle of the composite period. Earlier in the day, magnitudes would have been greater, whereas later in the day they would have been smaller. The change in magnitude of the divergence over the entire period of the afternoon composite as a result of system expansion is estimated to have been ~4% (see Appendix).

Winds relative to the squall system were obtained by subtracting the motion of the squall line for the region containing an observation (Fig. 11) from the observed wind. The relative winds obtained are shown in the (c) panels of Figs. 12, 14, 15, 17 and 18. It should be noted that these relative winds were not used in the calculation of divergence.

8. Low-level winds

Surface data and data from the US DC-6 aircraft (Table 1), which flew at 997 mb (152 m), were combined to yield a single low-level map with a high density of data plotted relative to the composite line. Streamlines, isotachs, relative winds and divergence are shown in Fig. 12. The streamlines were drawn for the map containing winds at both levels. The isotachs were determined by averaging grid-point values from separate isotach analyses for the two levels.

As the squall line progressed west-northwestward, it encountered north-northeasterly winds in the pre-squall environment (Fig. 12a), resulting in a strong relative flow of low-level environmental air directly toward the squall line (Fig. 12c). Strong convergence occurred along the line (Fig. 12d), and relative flow in a narrow zone just behind it was directed toward a gust front (Fig. 12c). The gust front was strong at the 400 m level, where it was encountered by the L-188 aircraft (Fig. 13; see also Reed, 1975).

Just behind the zone of convergence associated with the gust front was a parallel narrow zone of divergence, apparently associated with concentrated downdraft motion under the mature and dissipating convective cells located in the middle to rear of the convective zone (Fig. 12d). Weaker divergence prevailed throughout the remainder of the post-squall region.

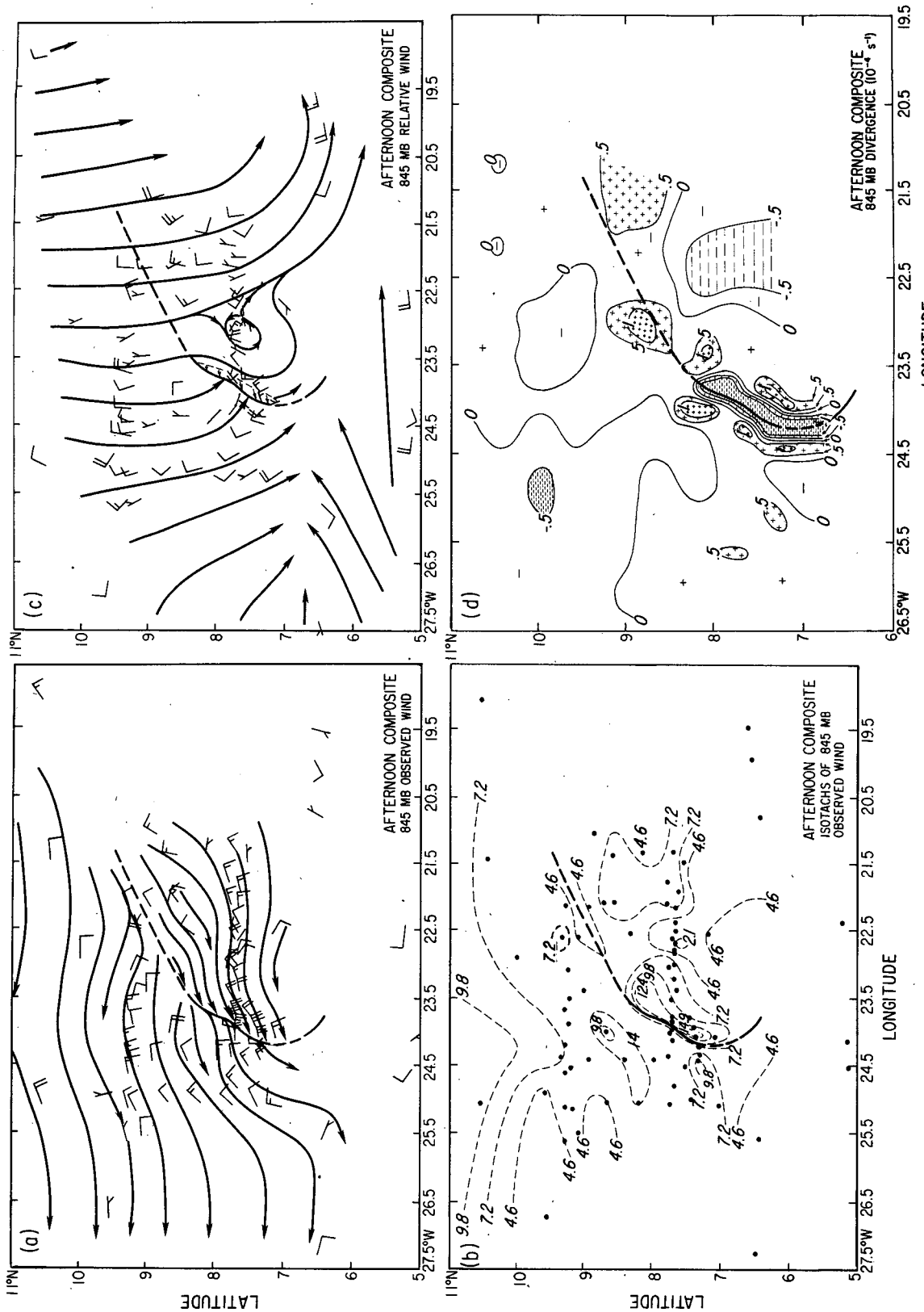

FIG. 14. As in Fig. 12, except for 845 mb. Types of observations are not indicated.

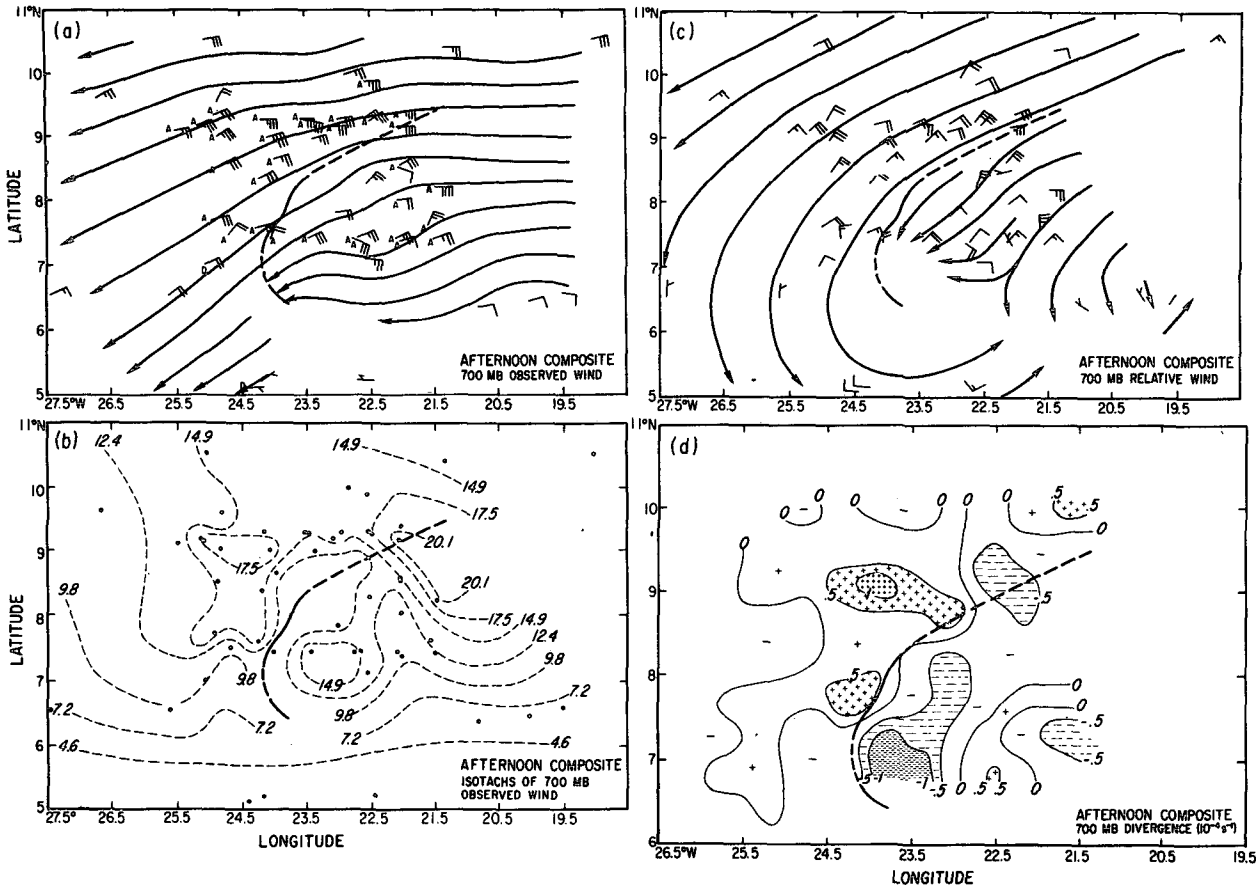

FIG. 15. As in Fig. 12, except for 700 mb.

9. Winds at 845 mb

At 845 mb moderate east to northeasterly winds prevailed just ahead of the squall line, with a narrow zone of strong easterlies just behind the line (Figs. 14a, b). Subtraction of the squall-line velocity shows that the relative flow at this level was toward the line both in the pre-squall environment and in a narrow zone just behind the line (Fig. 14c). Associated with this pattern was a zone of convergence paralleling the well-defined leading portion of the squall line (Fig. 12d). This convergence probably fed the downdrafts and updrafts of active convective cells along the line. An organized divergence pattern was absent along the weak northeastern extension of the squall line. A zone of weak to moderate divergence was located just to the rear of and parallel to the zone of strong squall-line convergence. The divergence here was probably associated with the mesoscale downdraft of the trailing transition and stratiform precipitation regions (further discussions of these regions are in Sections 17 and 18). A cyclonic vortex in the relative flow coincided roughly with this trailing divergence zone (Fig. 14c). The tendency of a vortex to form in trailing stratiform regions has been noted in other GATE squall lines (Houze, 1977; Fortune, 1980; Gamache and Houze, 1982); however, the vortex is usually seen at a higher level (650–700 mb).

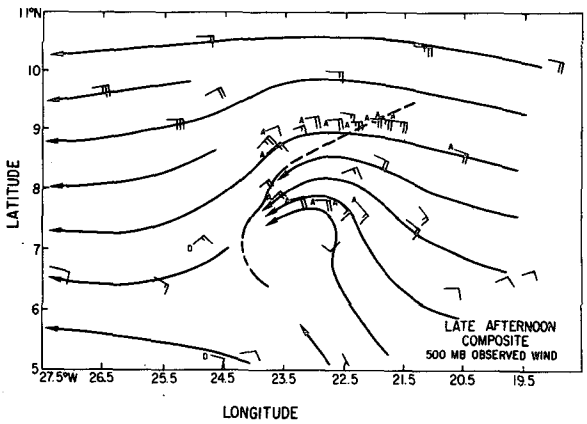

FIG. 16. As in Fig. 12a, except for 500 mb. Aircraft winds (indicated by A) are from the 1700–1830 GMT flight of the US C-130; therefore, this map is referred to as a "late" afternoon composite.

10. Winds at 700 mb

At 700 mb, the squall system was superimposed on a basic current consisting of the northeasterly flow ahead of a large-scale easterly wave (Fig. 15a). The isotach pattern (Fig. 15b), together with the relative flow (Fig. 15c), suggests a mesoscale intrusion of high-momentum air from the northeast into the post-squall region. Low-momentum air along the squall line separated zones of higher momentum in the pre- and post-squall regions.

The band of high momentum air in the latter region was evidently subsiding; it lay over the band of 845 mb divergence associated with the post-squall mesoscale downdraft (Fig. 14d). Perhaps the narrow zone of rear-to-front flow seen just behind the squall line at 845 mb (Fig. 14c) was the lower-level extension of this intruding and sinking high-momentum air. As noted in Section 9, the high momentum air at 845 mb was evidently converging into convective downdrafts located along the squall line. At 700 mb, the flow was generally convergent in the post-squall region (Fig. 15d).

11. Winds at 500 mb

A 500 mb streamline analysis based on sounding data and flight-level data from a late afternoon (1700–1840 GMT) flight of the US C-130 aircraft is shown in Fig. 16. Because the flight data were obtained after the period of the afternoon composite (~1200–1700 GMT; see Fig. 10), this analysis is referred to as a "late afternoon" composite and is not used in calculations of divergence and vorticity profiles discussed later in the paper. It is presented primarily as confirmatory evidence, showing that the data at this level were consistent with the analyses presented for other levels. The late afternoon 500 mb streamline pattern is clearly intermediate between those seen earlier in the day at 700 mb (Fig. 15) and 400 mb (Fig. 17). In addition to indicating vertical consistency, the similarity of the earlier and later patterns lends support to our application of a steady state assumption.

12. Winds at 400 mb

At 400 mb, an abrupt change in wind direction and speed occurred across the squall line (Figs. 17a, b). As

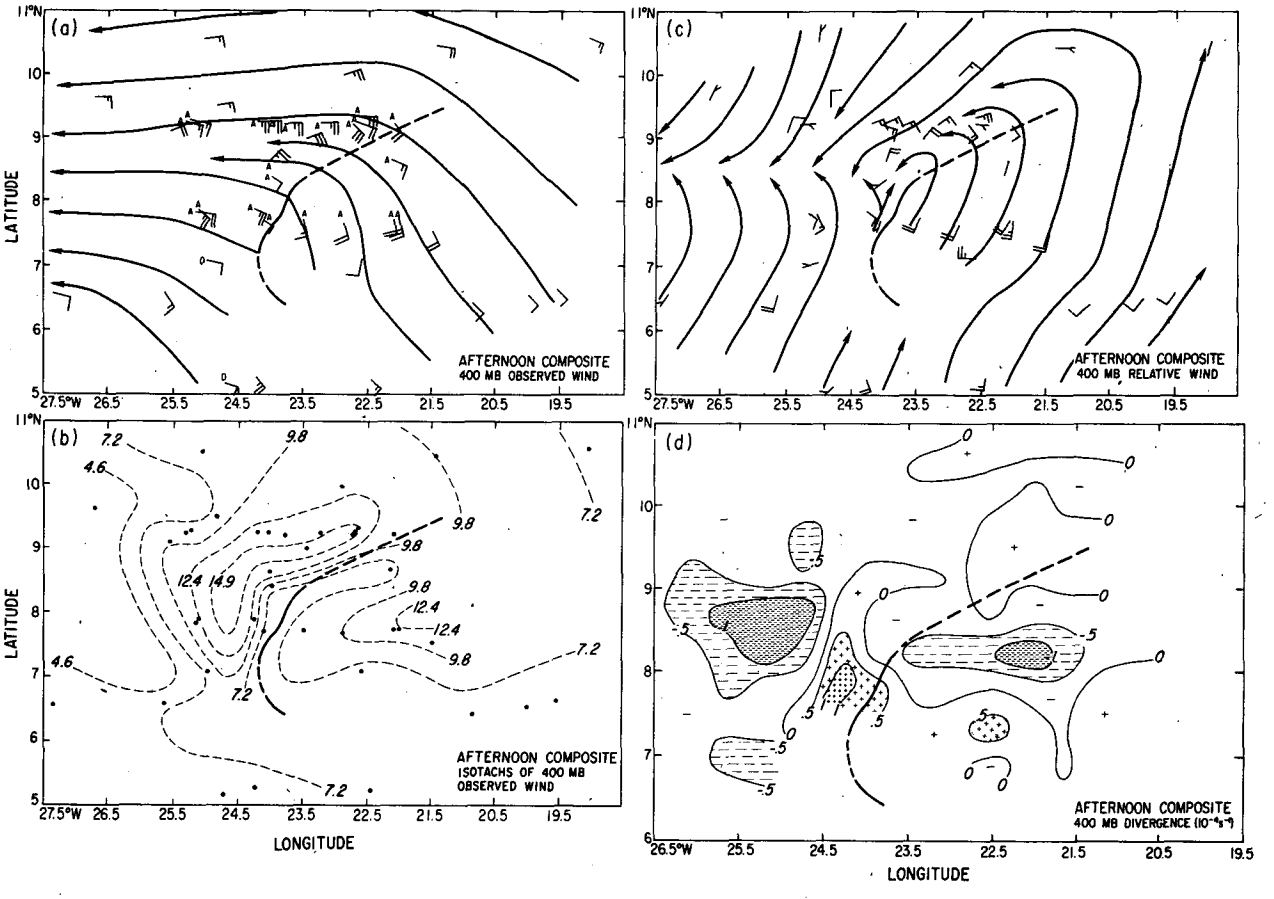

FIG. 17. As in Fig. 12, except for 400 mb.

at 700 mb, a band of weaker winds along the squall separated the pre-and post-squall regimes (cf. Figs. 15b and 17b). The relative wind pattern at 400 mb, however, was quite different from that at 700 mb (cf. Figs. 15c and 17c). At 400 mb, the relative flow in the central portion of the post-squall region was from the southwest, parallel to the squall line. In the northern portion of the post-squall region, this flow turned cyclonically and crossed the weaker northern part of the squall line. Although temporal irregularities in the squall-line motion, not taken into account in the composite analysis, could have produced transient episodes of front-to-rear relative flow across the line during the period of the composite, generally this squall was quite unlike the two GATE oceanic squall lines studied by Houze (1977), Zipser (1977) and Gamache and Houze (1982, 1983) in that there was no evidence of persistent strong front-to-rear flow across the squall line at this level, except at its southern end.

The 400 mb winds were convergent in the central-northern portion of the post-squall region (Fig. 17d). In the southwestern portion of the region, too few data were available to be confident of the divergence pattern.

13. Winds at 240 mb

At 240 mb, the winds were diffluent over the southern end of the line, while strong speed divergence was occurring over the central to northern parts (Figs. 18a, b). Divergence was centered over the squall line (Fig. 18d). The relative flow (Fig. 18c) was dominated by anticyclonic outflow covering most of the post-squall area, with air circulating outward across the squall line and streaming northwestward. Anticyclonic outflow over the post-squall stratiform region was also seen in the two oceanic GATE squall lines studied by Houze (1977), Zipser (1977) and Gamache and Houze (1982, 1983).

14. Regions of divergence and vertical motion analysis

The vertical distributions of horizontal divergence and vertical velocity within four types of regions within the squall system (see Fig. 19) were determined from the composite wind patterns just described. Two of these regions were parallel to SL. The first, called the *convective region,* enclosed the region of strongest low-

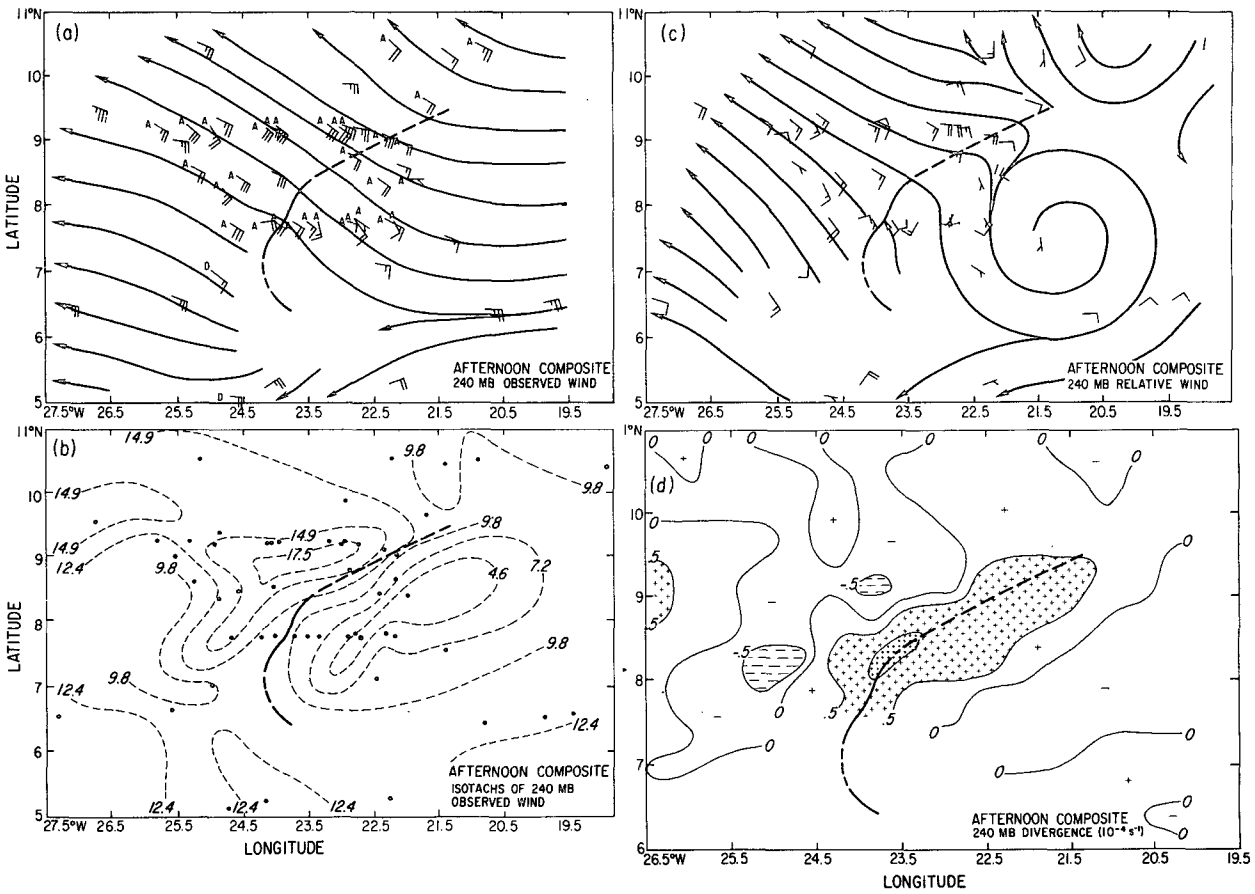

FIG. 18. As in Fig. 12, except for 240 mb.

level convergence. It covered the region between the line of pre-squall low-level divergences of -10^{-4} s^{-1} (Fig. 12d) and the isopleth of zero low-level divergence located 10–25 km behind the squall line. This region was 7.5×10^3 km^2 in area and is assumed to represent the zone of low-level convergence feeding the convective cells along the squall line. Justification for this interpretation is strengthened by observation that the back edge of the convective region roughly corresponded to a line 18 km behind and parallel to SL (Fig. 19); a distance of 18 km represents the mean width of the convective precipitation zone indicated by Fig. 7 (Section 6) for the afternoon composite period.

The line of zero low-level divergence (back edge of the convective region) formed the leading edge of the second region parallel to the squall line, the *transition zone.* The trailing boundary of the transition zone was a line connecting the back edges of the three areas of divergence greater than 10^{-4} s^{-1} seen in Fig. 12d. The transition zone thus covered the region of strongest low-level divergence. The precipitation characteristics in this region were typically intermediate between convective and stratiform. The transition zone covered 4.8×10^3 km^2.

Stratiform regions were defined with the aid of vertical cross sections from the early (1215), middle (1400) and late (1600) parts of the afternoon composite period. A stratiform rain area was identified by first locating any region in vertical cross sections that either had

- a bright band at the melting level or possessed the following characteristics:
- small horizontal gradients of reflectivity [less than about 1 dB(Z) km^{-1}],
- no low-level reflectivities greater than 38 dB(Z),
- uniform echo tops of less than about 11 km,
- no vertically oriented echo cores extending above about 5 km. Application of the latter two criteria was subjective in places.

The stratiform regions at 1215, 1400 and 1600 were extensive (some had areas exceeding 10^4 km^2) and generally easy to identify. They were located ahead of the squall line or behind the back edge of the convective zone described in Section 6. The areas of stratiform rainfall at 1215, 1400 and 1600 were replotted relative to the composite squall line. The union of 1) the stratiform area of 1400 that intersected that at 1215, and 2) the stratiform area at 1400 that intersected that at 1600, made up the final stratiform region shown in Fig. 19. This combined region was the most persistent area of stratiform precipitation characteristics, i.e., where few fluctuations in reflectivity occurred over periods of 2 h. None of the pre-line stratiform precipitation was persistent enough to be included in this combined region. To emphasize this fact we will refer to the combined regions as the *trailing stratiform region.* The trailing stratiform region was centered in the post-squall area and covered 1.3×10^4 km^2. Approximately 18% of the trailing stratiform region overlapped the transition zone.

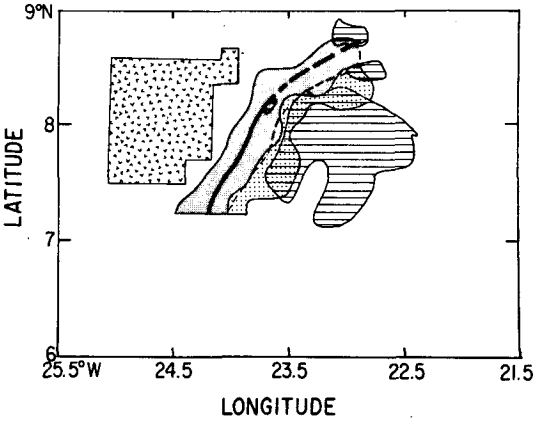

FIG. 19. Regions of divergence and vertical velocity calculations: convective region (gray), transition region (stippled), trailing stratiform region (hatched), and pre-line region (V's). Solid line is composite squall line. Thin dashed line represents mean back edge of convective echoes determined from Fig. 7.

Pre-line was the name given to the fourth region. As shown in Fig. 19, the pre-line area was essentially a mirror image of the trailing stratiform region, entirely ahead of SL, and covered 1.3×10^4 km^2.

15. Method of computing divergence and vertical velocity

Average divergences were determined in 50 km $\times$ 50 km grid squares in the low-level, 845, 700, 400 and 240 mb analyses shown in Figs. 12d, 14d, 15d, 17d and 18d, with resolution increased to 25 km $\times$ 25 km within 75 km of the composite squall line on the low-level and 845 mb maps. A pressure of 1005 mb was assigned to the low-level analysis, which was composed of a combination of 1012 mb surface data and 997 mb flight data. The mean divergence for each of the four regions in Fig. 19 was determined at each analysis level by averaging the individual grid-square values in each region. The technique of Gamache and Houze (1982) was then used to obtain the vertical profiles of divergence and vertical motion (ω, in mb h^{-1}) in each region. According to their methods, a polynomial fit was used to obtain a continuous vertical distribution of divergence up to 150 mb. These smooth divergence profiles were modified by assuming that errors in divergence increased linearly with decreasing pressure (following O'Brien, 1970) and that $\omega = 0$ at 150 mb.

16. Divergence profiles

Divergence profiles for the convective, transition, trailing stratiform and pre-line regions are shown in Fig. 20. The convective region (Fig. 20a) was conver-

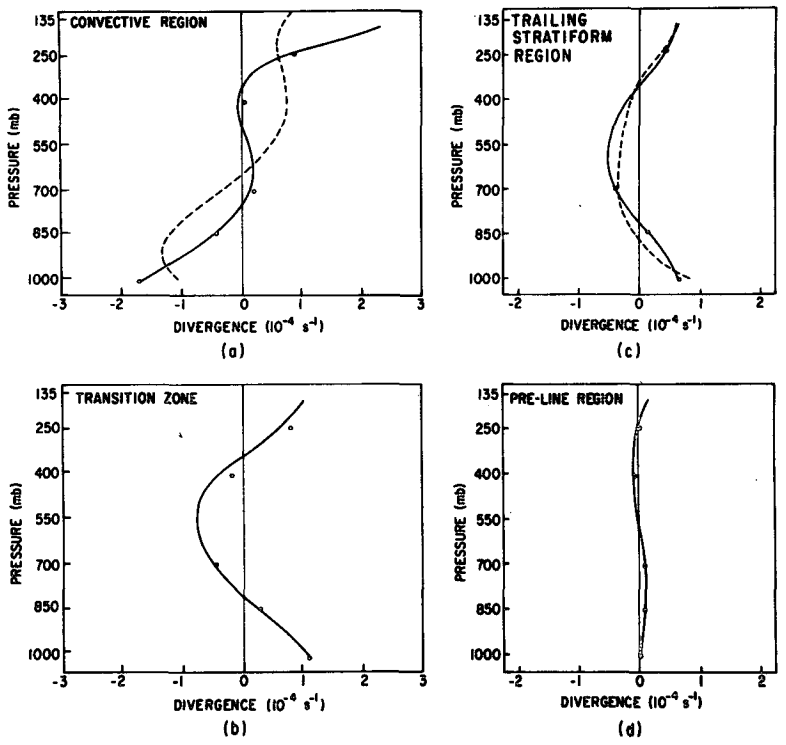

FIG. 20. Mass balanced profiles of average divergence in the (a) convective, (b) transition, (c) trailing stratiform and (d) pre-line regions of the squall system. Circles indicate data points before mass balancing. Dashed profiles are those of Gamache and Houze (1982).

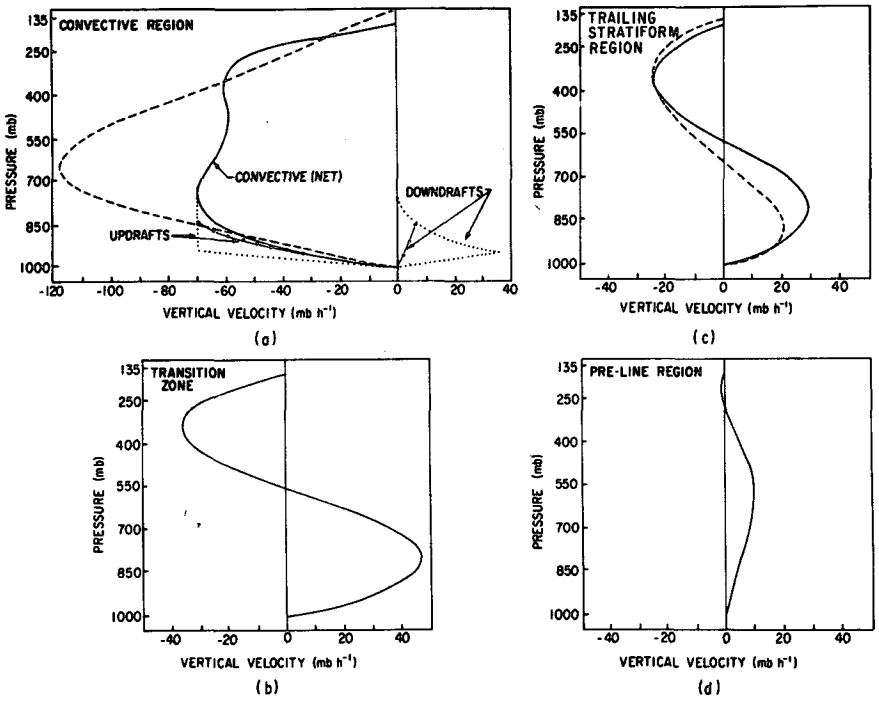

FIG. 21. Profiles of average vertical velocity in the (a) convective, (b) transition, (c) trailing stratiform and (d) pre-line regions of the squall system. In (a) and (b), dashed line shows net convective vertical motion determined by Gamache and Houze (1982). Decomposition of our net convective curve into updraft and downdraft components is indicated for two sets of assumptions: dotted lines assume that unmodified environment air is entrained into the updrafts and downdrafts; the circle-dash lines assume that the environment air is lifted on the mesoscale prior to being entrained (see text).

gent throughout the layer from 1005 to 750 mb, nondivergent between 750 and 350 mb and divergent above. This profile is similar to that obtained by Gamache and Houze (1982) (also shown in Fig. 20a). Both profiles show convergence at lower levels and divergence at upper levels; however, the layer of divergence at upper levels was deeper in their case, extending from 650 to 100 mb.

The profiles of divergence in the transition and trailing stratiform regions (Figs. 20b, c) were fundamentally different from that in the convective region. Convergence occurred only in midlevels, with divergence at upper and lower levels. The profile in the trailing stratiform region agrees well with the stratiform region profile obtained by Gamache and Houze (1982). The profile in the transition zone had the same shape as that in the trailing stratiform region, but greater intensity.

17. Vertical motion profiles

Profiles of vertical velocity in the four regions of the composite system are presented in Fig. 21. In the convective region (Fig. 21a), net upward motion was found at all levels. The magnitude of the net vertical velocity, however, was only about half of that determined by Gamache and Houze (1982).

Using a procedure similar to that used by Gamache and Houze (1982), we decomposed the net upward motion in the convective region into updraft and downdraft contributions. According to their procedure, we first reviewed pre-line soundings obtained in undisturbed areas. These soundings indicated that only parcels originating below about 950 mb could have risen to upper levels. If convergence between 950 mb and the level of maximum ascent (750 mb) is then assumed to maintain convective downdrafts and if downdrafts are initiated at 750 mb, become strongest at 950 mb and decrease linearly to zero at the surface, then a downdraft vertical profile can be obtained by integrating downward from 750 to 950 mb and then linearly interpolating between 950 mb and the surface. Next the downdraft profile can be subtracted from the net vertical motion profile to obtain a convective updraft profile. The convective updraft and downdraft vertical velocity obtained in this way are included in Fig. 21a. Further inspection of pre-line soundings indicated that if they were destabilized by a moderate amount of mesoscale lifting, buoyant parcels originating below 800–850 mb could have reached the upper troposphere. Therefore, the vertical motions within the convective region were recalculated, assuming that all convergence below 845 mb supported convective updrafts, while convergence between 750 and 845 mb maintained convective downdrafts. The profiles obtained in this way appear as dash–circle lines in Fig. 21a. The resulting strength of the convective downdraft in this case is much reduced from that of the unlifted soundings.

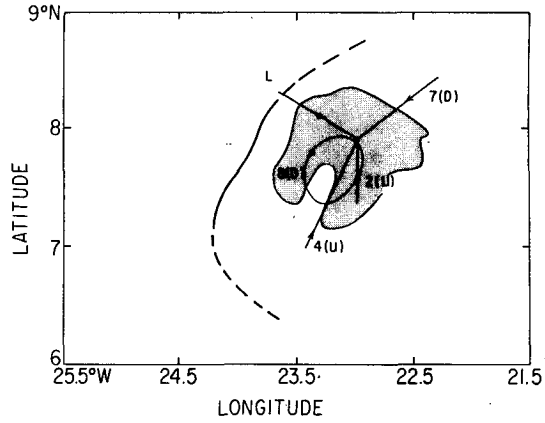

FIG. 22. Relative flow into the post-squall stratiform precipitation area (shaded). Vectors show relative flow trajectories (3 h displacements) into a point at the center of the region at low levels (L), 700 (7), 400 (4) and 240 (2) mb. The closed streamline indicates the relative flow at 845 (8) mb. The vectors and streamlines are based on analyses in Figs. 12c, 14c, 15c, 17c and 18c. Letters in parentheses indicate whether the level was characterized by mesoscale updraft (U) or mesoscale downdraft (D). The heavy line indicates the squall-line position.

The vertical velocity profiles for the transition zone and the trailing stratiform region are similar, with the intensity of the vertical motions greater in the transition zone than in the trailing stratiform region (Figs. 21b, c). These regions are characterized by mesoscale updraft motion at mid to upper levels and mesoscale downdraft motion at mid- to lower levels. This profile agrees well with the stratiform region profile obtained by Gamache and Houze (1982), except that the level of zero vertical motion separating the mesoscale updraft aloft from the downdraft below in our case was at 580 mb, whereas theirs was at about 650 mb. Johnson (1982) found zero vertical motion at about 500 mb in a nonsquall tropical cloud cluster, while Ogura and Liou (1980) found zero vertical motion at the 600 mb level in the trailing stratiform region of a midlatitude squall line.[6]

Weak subsidence occurred throughout the lower and midtroposphere in the pre-line sector (Fig. 21d). This subsidence may have been induced by evaporation of precipitation falling from the pre-line echo overhang; it may have been produced to compensate partially the upward motion in the squall system, or it may have been due to the large-scale circulation rather than directly related to the dynamics of the squall line. The layer from 300 to 150 mb had very weak upward motion. The upward motion in this region (although miniscule) is consistent with the existence of the weakening pre-line anvil in that region.

[6] The 0°C level in our case as well as Gamache and Houze's and Ogura and Liou's was at about 600 mb, while in Johnson's case it was slightly higher, between 550 and 600 mb.

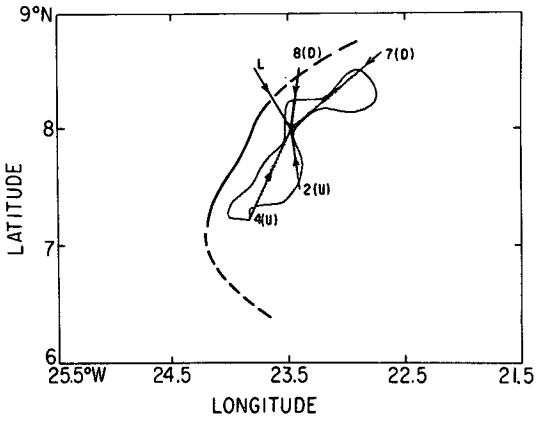

FIG. 23. Relative flow into the transition zone (shaded). Vectors show relative flow trajectories (3 h displacements) into a point at the center of the region at low levels (L), 845 (8), 700 (7), 400 (4), and 240 (2) mb. Letters in parentheses indicate whether the level was characterized by mesoscale updraft (U) or mesoscale downdraft (D). Flow vectors are based on Figs. 12c, 14c, 15c, 17c and 18c.

18. Relationship of the pre- and post-squall stratiform precipitation areas to the relative airflow

In this section, we examine the relationship of the pre- and post-squall stratiform precipitation areas to the relative flow documented in preceding sections. The relative flow into the post-squall stratiform area (the trailing region for which the mesoscale vertical motions in Fig. 21c were determined) is shown in Fig. 22. At low levels, air was streaming into the region from the rear of the convective region, in a manner similar to other GATE oceanic squall systems (e.g., Fig. 5b of Gamache and Houze, 1982).

At 845 mb air was circulating cyclonically within the trailing stratiform region and subsiding, while at 700 mb air was entering the region from the northeast. Since little convective activity was occurring to the northeast, the air entering from that direction was probably unsaturated and therefore susceptible to evaporative cooling. On entering the trailing stratiform region from the northeast, this air became part of the mesoscale downdraft.

At 400 and 240 mb the relative flow seen in Fig. 22 was quite different from the flow at lower levels; it entered the trailing stratiform region from the south and fed the mesoscale updraft. In other GATE oceanic squall systems, the relative flow at these levels has also been seen to feed the mesoscale updraft; however, it enters the region with a strong front-to-rear component across the squall line (e.g., Figs. 7c and 8c of Gamache and Houze, 1982). This front-to-rear component normal to the squall line carries hydrometeors and air of high moist static energy from the convective region into the upper levels of the stratiform region (Gamache and Houze, 1983). Although the relative flow at 400–240 mb in our case was from the south rather than perpendicular to the squall line, the flow was arriving from a region where the southern end of the squall line was interacting throughout the day with other convective systems [see Rappaport (1982) for a detailed description of this interaction]. Thus, as in the more typical squall system, the flow at upper levels evidently was transporting hydrometeors and high moist static energy into the stratiform mesoscale updraft region; however, in this case, the transport was from a different convective region.

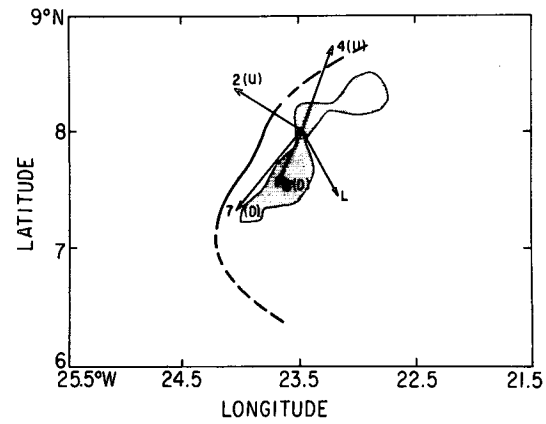

FIG. 24. Relative flow out of the transition zone (shaded). Vectors show relative flow trajectories away from a point at the center of the region at low levels (L), 845 (8), 700 (7), 400 (4) and 240 (2) mb. Letters indicate whether the level was characterized by mesoscale updraft (U) or downdraft (D). Flow vectors are based on Figs. 12c, 14c, 15c, 17c and 18c.

The relative flow in the transition zone at the rear of the squall line is summarized in Figs. 23 and 24. Since the relative flow in this region (Figs. 12c, 14c, 15c, 17c and 18c) exhibited considerable curvature at some levels, two diagrams were constructed; Fig. 23 shows the flow into the transition zone while Fig. 24 shows the flow away from the region. The relative flow into the transition zone (Fig. 23) generally resembled the flow into the trailing stratiform region, except at 845 mb the flow was not circulating within the region but rather flowing in from the north. Thus, as in the trailing stratiform region, the downdraft in the transition zone was being fed by lower tropospheric air from the north to northeast, whereas the updraft was being fed by upper tropospheric (400–240 mb) flow from the south.

The relative flow away from the transition zone (Fig. 24) was streaming toward the rear of the system into the trailing stratiform region at low levels. However, the subsiding relative flow at 700–845 mb was nearly parallel to the squall line and thus remained in the transition zone or flowed into the rear of the convective region behind the bulge in the southern end of the line.

The flow out of the transition zone at upper levels (400–240 mb in Fig. 24) tended to be directed across the squall line, into the pre-line region. This tendency

evidently accounts for the formation of the upper-level echo overhang and stratiform precipitation ahead of the squall line. We further note that this pre-line radar-echo feature was rather transient (recall Figs. 2 and 3). The relative flow on which Fig. 24 is based, however, was determined by a composite analysis, which preserved the persistent rather than the transient character of the flow. We suggest that during the time that the pre-line precipitation became most pronounced the tendency for rear-to-front relative flow across the line at upper levels was temporarily stronger than that shown by the composite analysis.

In Section 6, it was noted that the stratiform precipitation ahead of and behind the line combined to account for some 42% of the squall-line system's total precipitation, and that this fraction is similar to the fraction of total system precipitation accounted for by the single trailing stratiform precipitation areas of the two previously studied GATE oceanic squall-line systems. In those systems, the hydrometeors corresponding to those constituting the pre-line stratiform echo seen in our case were evidently advected strongly rearward, and the two stratiform echoes, seen separately in our case, were superimposed and thus seen as one entirely trailing stratiform precipitation region. The apparent separation of the upper portion of the stratiform radar echo from the lower portion by the relative flow aloft in our case is consistent with the echo cross sections discussed in Section 4, where it was seen that the stratiform precipitation ahead of the squall line developed in association with a radar-echo overhang at upper levels (Figs. 3c–h), while the stratiform precipitation to the rear of the line was characterized by lower echo top (Figs. 3c–l).

From the foregoing discussion, the relationships of the pre- and post-squall precipitation areas to the squall-relative airflow may be summarized as follows. The pre-squall stratiform precipitation was apparently the result of forward advection of hydrometeors by the relative flow across the squall line at upper levels. No strong mesoscale updraft was detectable ahead of the squall line. The post-squall stratiform precipitation, on the other hand, was apparently maintained jointly by condensation produced by the mesoscale updraft (Fig. 21c) and advection of condensate from the south, where the end of the squall line was interacting with other convective systems.

It is possible that the tropical squall system studied here was somewhat self-destructive since the stratiform precipitation falling from the pre-line anvil would have tended to evaporate and cool the air ahead of the system. If mesoscale subsidence resulted from the cooling (recall the pre-line subsidence indicated by Fig. 21d), stabilization of the pre-line environment would have ensued, and premature weakening of the squall line would have set in. This scenario would have been consistent with the fact that the convective cells in the line steadily weakened after the appearance of the pre-line stratiform echo (see Figs. 3d–l and 7; also note the coincidence in timing of the beginning of AL in Fig. 8a and the occurrence of the minimum cloud top temperature in Fig. 9). However, the evidence for self-destructiveness in this case is not conclusive. As shown by Rappaport (1982), the northern part of the squall system begins to encounter lower surface moist static energy and sea-surface temperatures just before its demise.

19. Conclusions

The 28 June 1974 squall line over the GATE ship array exhibited convective and mesoscale vertical motions similar to the two GATE oceanic squall lines previously reported by Houze (1977), Zipser (1977) and Gamache and Houze (1982, 1983). The 28 June squall line exhibited regions of distinctly convective and stratiform precipitation, and, like the other two lines, nearly half (42%) of the total precipitation was stratiform.

Although the vertical air motions and the fractional amount of stratiform precipitation in this squall system resembled those of the two previously studied GATE oceanic squall lines, this line moved less rapidly than the other squall lines, and the relative horizontal flow through the system differed markedly from that of the other lines. This result confirms Hamilton and Archbold's (1945) speculation that tropical squall lines can occur with different relative horizontal flow patterns. Our study further confirms Hamilton and Archbold's conjecture that in the proper relative flow configuration upper-level cloud layers and precipitation may extend forward from the squall line. We find that such a forward cloud layer did in fact occur in our case and that a large portion of the stratiform precipitation actually fell ahead of the squall line, apparently as a result of condensate being advected forward of the line by the relative flow at mid to upper levels. Discrete line-element propagation, prevalent in some squall lines, was absent in this case. This difference apparently was associated with the line's slower speed, different relative airflow and pre-line overhang of precipitating cloud. The development of stratiform precipitation ahead of the line may have had a destructive effect on the evolution of the squall system, but our data are not conclusive on this point.

The relative horizontal flow in the case described here illustrates that two-dimensional reasoning, often used to explain the structure and behavior of squall lines in terms of wind components in a cross-section plane normal to the line, may sometimes be inadequate. While the relative flow responsible for the cloud and precipitation structure in the post-squall region of our case was normal to the squall line at the surface, it was generally parallel to the line and from the north at low to mid levels and generally parallel but from the south at mid to upper levels. The three-dimen-

sionality of our system, together with its other described differences from the two previously reported GATE oceanic squall lines, indicates that future theoretical analyses, numerical studies and conceptual modeling of tropical squall lines face a more difficult challenge than if these lines always exhibited two-dimensionality and great similarity from case to case.

Acknowledgments. The authors with to thank Dr. E. J. Zipser for his continued interest in this work and for the opportunity of visiting his research group at the National Center for Atmospheric Research. Dr. J. F. Gamache aided in the development of the various computer programs used in this study. The analysis in the Appendix was provided by D. D. Churchill. Dr. T. J. Matejka made valuable comments on this study. This research was supported by the National Science Foundation under Grant ATM80-17327. This paper is Contribution No. 675, Department of Atmospheric Sciences, University of Washington.

APPENDIX

Effect of Squall-line Expansion on Divergence Calculations

This paper describes a composite wind analysis in which data taken at various times are plotted by determining their spatial position in relation to the squall line and locating them on a common map in relation to the line's mean position during the period of analysis. This procedure assumes that the winds are in steady state in a coordinate system attached to the squall line. From Fig. 5, however, it is evident that the squall line expanded somewhat during the period of the composite. This expansion is represented ideally in Fig. A1 as an arc (defined by an angle $\Delta\theta$) expanding radially outward from a common origin (point P). The position of the squall line is shown at two times (t_1 and t_2). The line is assumed to move at constant speed. The four-sided figure labeled "abcd" at t_1 and "1234" at t_2 represents a portion (or subregion S) of the mesoscale system moving with the squall line. According to the steady-state assumption previously mentioned, the winds at the four corners of subregion S are identical at times t_1 and t_2. That is, we assume

$$\frac{d}{dt}\left[\frac{1}{L}\oint \mathbb{V}_n \cdot d\mathbb{l}\right] \equiv 0, \tag{A1}$$

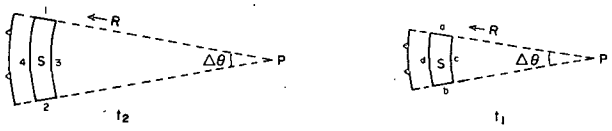

FIG. A1. Squall line (indicated by frontal symbol) and subregion S at two times (t_1 and t_2). Other symbols defined in text.

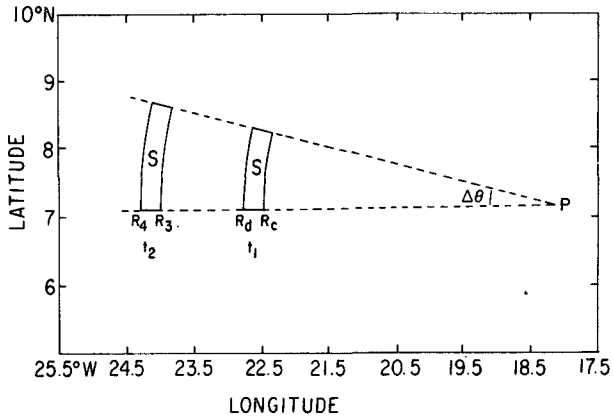

FIG. A2. A subregion S of the squall system at t_1 = 1200 GMT and t_2 = 1800 GMT (see text).

where the integral is taken around the perimeter of S, L is the length of the perimeter, $\mathbb{V}_n$ the component of the wind normal to the perimeter and $\mathbb{l}$ a unit vector tangent to the boundary. It follows that the wind divergence (div) over the subregion decreases from t_1 to t_2. The rate of change of div is given by

$$\frac{d}{dt}\,\mathrm{div} = \frac{d}{dt}\left[\frac{1}{A}\oint \mathbb{V}_n \cdot d\mathbb{l}\right]$$

$$= -A^{-2}\frac{dA}{dt}\oint \mathbb{V}_n \cdot d\mathbb{l} + A^{-1}\frac{d}{dt}\oint \mathbb{V}_n \cdot d\mathbb{l}. \tag{A2}$$

But from (A1), we have

$$\frac{d}{dt}\oint \mathbb{V}\cdot d\mathbb{l} = L^{-1}\frac{dL}{dt}\oint \mathbb{V}_n \cdot d\mathbb{l}. \tag{A3}$$

Substituting (A3) into (A2), and rearranging terms, we obtain

$$\frac{d[\ln(\mathrm{div})]}{dt} = \frac{d}{dt}\ln\left(\frac{L}{A}\right). \tag{A4}$$

Integrating (A4) with respect to t from t_1 to t_2 yields

$$\frac{\mathrm{div}(t_2)}{\mathrm{div}(t_1)} = \frac{L(t_2)}{L(t_1)}\cdot\frac{A(t_1)}{A(t_2)}. \tag{A5}$$

From Fig. A2, we obtain

$$\frac{\mathrm{div}(t_2)}{\mathrm{div}(t_1)} = 0.96,$$

indicating that the change in the magnitude of divergence resulting from system expansion during the afternoon was only about 4%.

REFERENCES

Churchill, D. D., and R. A. Houze, Jr., 1984: Development and structure of winter monsoon cloud clusters on 10 December 1978. *J. Atmos. Sci.*, **41** (in press).

Fortune, M., 1980: Properties of African disturbance lines inferred from time-lapse satellite imagery. *Mon. Wea. Rev.*, **108,** 153–168.

Gamache, J. F., and R. A. Houze, Jr., 1982: Mesoscale air motions associated with a tropical squall line. *Mon. Wea. Rev.*, **110,** 118–135.

——, and ——, 1983: Water budget of a mesoscale convective system in the tropics. *J. Atmos. Sci.*, **40,** 1835–1850.

Hamilton, R. A., and J. W. Archbold, 1945: Meteorology of Nigeria and adjacent territory. *Quart. J. Roy. Meteor. Soc.*, **71,** 231–262.

Houze, R. A., Jr., 1977: Structure and dynamics of a tropical squall-line system. *Mon. Wea. Rev.*, **105,** 1540–1567.

——, and A. K. Betts, 1981: Convection in GATE. *Rev. Geophys. Space Phys.*, **16,** 541–576.

Hudlow, M., R. Arkell, V. Patterson, P. Pytlowany, F. Richards and S. Geotis, 1979: Calibration and intercomparison of the GATE C-band weather radars. NOAA Tech. Rep. EDIS 31, NOAA, 98 pp. [NTIS PB81-120305 81-05 965].

Johnson, R. H., 1982: Vertical motion in near-equatorial winter monsoon convection. *J. Meteor. Soc. Japan,* **60,** 682–690.

Maddox, R. A., 1980: Mesoscale convective complexes. *Bull. Amer. Meteor. Soc.*, **61,** 1374–1387.

O'Brien, J. J., 1970: Alternate solutions to the classical vertical velocity problem. *J. Appl. Meteor.*, **9,** 197–203.

Ogura, Y., and M. T. Liou, 1980: The structure of a midlatitude squall line: A case study. *J. Atmos. Sci.*, **37,** 553–567.

Rappaport, E. N., 1982: Structure and dynamics of an atypical tropical squall-line system. M.S. thesis, University of Washington, 266 pp.

Reed, R. J., 1975: An example of a squall line in the B-scale network. *GATE Rep. No. 14,* Vol. 1, Int. Counc. of Sci. Unions, WMO, 217–222.

Smith, E. A., T. H. Vonder Haar and M. Whitcomb, 1979: GATE Satellite surface radiation data archives. Tech. Rep., Dep. of Atmos. Sci., Colorado State University, 210 pp.

Zipser, E. J., 1969: The role of organized unsaturated convective downdrafts in the structure and rapid decay of an equatorial disturbance. *J. Appl. Meteor.*, **8,** 799–814.

——, 1977: Mesoscale and convective-scale downdrafts as distinct components of squall-line circulation. *Mon. Wea. Rev.*, **105,** 1568–1569.